IEICE TRANS. COMMUN., VOL.E94–B, NO.5 MAY 2011

INVITED PAPER *Special Section on Antenna and Propagation Technologies Contributing to Diversification of Wireless Technologies*

RF Propagation and Channel Modeling for UWB Wearable Devices

Kamya YEKEH YAZDANDOOST[†a)], **Kamran SAYRAFIAN-POUR**[††], *Nonmembers*, *and* **Kiyoshi HAMAGUCHI**[†], *Member*

SUMMARY Wireless body area network for sensing and monitoring of vital signs is the one of most rapidly growing wireless communication system and Ultra Wide-Band (UWB) is a favorable technology for wearable medical sensors. The wireless body area networks promise to revolutionize health monitoring. However, designers of such systems face a number of challenging tasks. Efficient transceiver design requires in-depth understanding of the propagation media which in this case is the human body surface. The human body is not an ideal medium for RF wave transmission; it is partially conductive and consists of materials of different dielectric constants, thickness and characteristic impedance. The results of the few measurement experiments in recent publications point to varying conclusions in the derived parameters of the channel model. As obtaining large amount of data for many scenarios and use-cases is difficult for this channel, a detailed simulation platform can be extremely beneficial in highlighting the propagation behavior of the body surface and determining the best scenarios for limited physical measurements. In this paper, an immersive visualization environment is presented, which is used as a scientific instrument that gives us the ability to observe three-dimensional RF propagation from wearable medical sensors around a human body. We have used this virtual environment to further study UWB channels over the surface of a human body. Parameters of a simple statistical path-loss model and their sensitivity to frequency and the location of the sensors on the body are discussed.

key words: *UWB antenna, immersive visualization system, channel model, body area network*

1. Introduction

The range of medical devices that are being used on or inside the human body is expected to significantly increase in the near future. Recent advances in microelectronics indicate that the technology to achieve ultra-small and ultra low power wearable devices is mostly available. The wireless body area network is of special interest in for sensing and monitoring applications in healthcare. Communications from in-body implants and on-body sensors will allow for better diagnoses and improvement in therapy. However, numerous challenges including size, cost, energy source, sensing/actuator technology, transceiver design still need to be resolved [1]. RF-enabled wearable sensor nodes offer an attractive set of applications, among which we can point to Electrocardiogram (ECG), various medical monitoring applications such as Temperature, Respiration, Heart rate, Blood pressure and pH.

The Ultra-Wideband (UWB) technology with its advantages over narrow-band systems is a possible candidate technology for body area network [2] having a radio spectrum that is almost universally available. A successful design in body area networks should accommodate mobility, sensitivity [3], compact size and light weight. Although, factors such as interference and co-existence with other wireless technologies are extremely important in the choice for BAN operating frequency, worldwide availability and also the opportunity to have reasonable sized antennas make UWB an attractive candidate for wearable BAN applications.

A key component of wireless body area network is an antenna. It must meet both biocompatible and size-limitation requirements. Therefore, designing proper antennas for wireless body area network is a challenging task. Also, compare to the traditional antennas, it is more complicated to provide the typical parameters such as bandwidth, efficiency and gain within the limited antenna volume. So, the antenna design becomes even more critical at UWB frequencies. Moreover, such antennas for the UWB system should have linear polarization, omni-directional patterns, and constant gain. Therefore, UWB antenna for wireless body area network should be designed carefully to avoid unnecessary distortions [4]. Consideration of the antenna characteristics influenced by the human body is very important for the antenna design [5].

Efficient transceiver design requires in-depth understanding of the propagation medium which in this case is human body surface. The results of the few measurement experiments in recent publications point to varying conclusions in the derived parameters of the channel model. For example, authors in [6] perform measurement between a receiver node located on the stomach and 9 transmitter nodes that are placed around the front-upper side of the body. Their obtained average path loss exponent for UWB is around 0.84. Authors in [7] conduct measurement around the human torso in various parallel planes and obtain a path-loss exponent of around 5.8. Path loss exponents of around 3 have also been reported when measurements are performed in front of the torso [8], [9]. These discrepancies simply point to the need for more detailed studies in order to understand the behavior of Radio Frequency (RF) waves over the human body surface.

As obtaining large amount of data for many scenarios

Manuscript received August 13, 2010.
Manuscript revised November 17, 2010.

[†]The authors are with National Institute of Information and Communications Technology (NICT), Yokosuka-shi, 239-0847 Japan.
[††]The author is with National Institute of Standards and Technology, Gaithersburg, Maryland, USA.
a) E-mail: yazdandoost@nict.go.jp

DOI: 10.1587/transcom.E94.B.1126

and use-cases for this channel is difficult, a platform that can emulate physical experiments in a three-dimensional (3D) virtual reality environment can be extremely beneficial in highlighting the propagation behavior of the body surface; and also determining the best scenarios for limited physical measurements. Lack of a detailed human body model and a realistic wearable antenna are usually among the shortcomings of previous simulation studies in this area.

In this paper, we use a state of the art 3D virtual reality simulation platform to study electromagnetic propagation from wearable sensors. Communication with a wearable device can be done from any direction inside, outside or over the surface of the body due to various body postures and human motion. Consequently, a true 3D environment is needed to better capture, visualize and understand RF propagation for such devices. In the following sections, we describe such a platform and show how it can be used to extract a simple statistical path-loss model for body surface communication.

The rest of this paper is as follows. The antennas used in our simulations are discussed in Sect. 2. Section 3 will describe the immersive 3D platform that we have constructed to study RF propagation from wearable sensors. Then, description of the simulated scenarios and our results are provided in Sect. 4. Finally concluding remarks are expressed in Sect. 5.

2. UWB Antenna

Printed monopole and dipole antennas are extensively used in different wireless applications due to their many advantages, such as low profile, light weight, easy to fabricate and low cost [10], [11].

The loop antennas also can be used for wireless communications [12]–[14]. However, a conventional wire loop antenna shows less than 10% bandwidth for a 2:1VSWR. Therefore, conventional loop antenna has went under different modifications to increase the bandwidth. A broadband loop antenna introduced in [12], has a small gap in the wire loop. This small gap increases the impedance bandwidth to more than 24%.

In our study we used a loop antenna whose left and upper arms together introduce an L-shape [15]. However, the L-shape antenna itself is a class of broadband planar antenna, which allows the broad impedance bandwidth and less cross-polarization radiation [16], [17].

The structure of L-loop antenna is illustrated in Fig. 1. To have a linearly polarized radiation the total length of outer limits of the square loop antenna should be equal to one wavelength [18].

The wavelength λ_0 for an antenna designed at 3.1 GHz is 96.77 mm. Our proposed antenna is composed of a single metallic layer and is printed on a side of a FR4 substrate with dielectric constant of $\varepsilon_r = 4.4$, loss tangent of $\tan\delta = 0.02$, and thickness of 1 mm. A coupled tapered transmission line is printed in the same side with similar metallic layer. A copper of 0.018 mm thickness has been used as a metallic

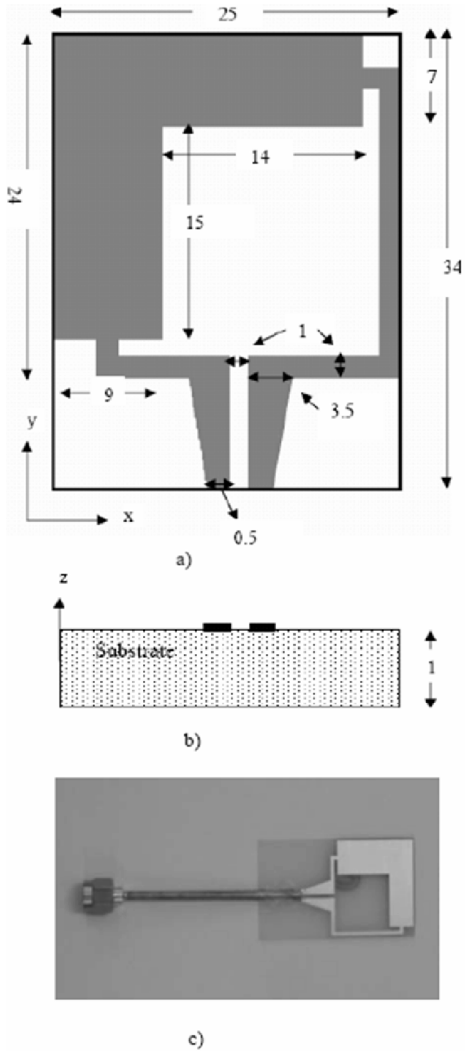

Fig. 1 (a) Top view, (b) Side view, (c) Prototype of the antenna structure (Unit: mm).

layer. As shown in Fig. 1 the size of the proposed antenna is $24 \times 25 \times 1$ mm, which is quite appropriate for wireless system. The rectangular loop has 98 mm length, which is fairly close to one wavelength of designed antenna. In this work we used taper transmission line for impedance matching, and we modified the shape of conventional loop antenna with introducing an L portion to its arms, as shown in Fig. 1, to reduce the antenna internal reflections at its discontinuities and make gradual transition between the metal surface of the antenna and free space. The broadband characteristics of the proposed antenna can be understood by its current distribution as the current is relatively more distributed over the antenna L portion.

The antenna is fed from a 50 Ohms connector through a coupled tapered transmission line. The tapered transmission lines have shown good impedance matching over a wide range of frequency [19]–[24]. The geometry of the taper is chosen to minimize the reflection and optimize impedance matching and bandwidth. A tapered structure in

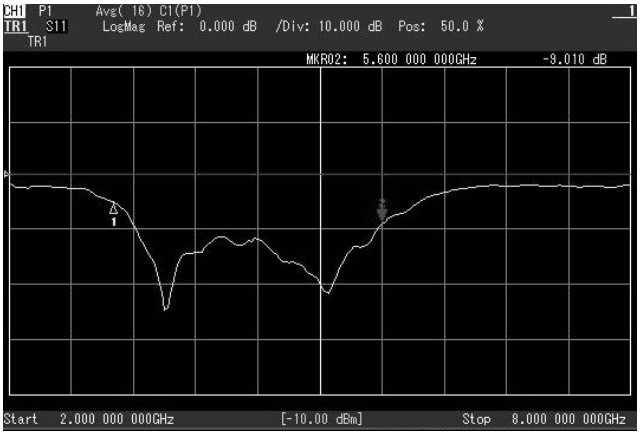

Fig. 2 Measured S_{11} of the antenna.

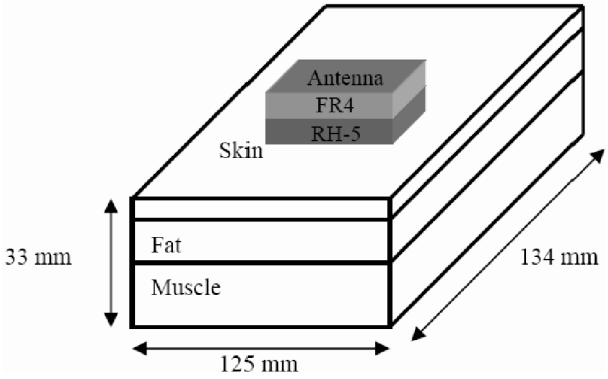

Fig. 3 Antenna on the proximity of body tissues.

the feed area creates low current standing wave ratios, therefore more magnitude of pulse near to the feed point. The measured S_{11} of antenna is shown in Fig. 2.

In order for an antenna to be suitable for wearable body area applications, it should be placed near to the body with a sufficient separation from the surface. The simulation results are shown that a minimum separation of 14 mm is necessary to reduce the effect of the human body on the antenna characteristics [25]. Therefore, in our work we added a second layer substrate i.e. RH-5 [26] with thickness of 14 mm, $\varepsilon_r = 1.09$ and $\tan\delta = 0.0004$, as shown in Fig. 3. This substrate is chosen due to its relative permittivity, which is close to air and therefore it will not affect the antenna parameters. As a result the same antenna can be used for on-body and away from body as well.

A model of a human body consisting of three layers (i.e. skin, fat, and muscle) has been used to study the effects of human body on antenna characteristics as shown in Fig. 3. The dimensions are 134×125×33 mm. The total thickness is 33 mm, which consists of three layers: 1 mm skin, 2 mm fat, and 30 mm muscle. The effect of blood vessels, sweat gland, and any form of water-content tissues are not considered in this simulation.

The electrical properties of human body tissues i.e. skin, fat, and muscle at 4.1 GHz are shown in Table 1. The calculation of electrical properties is based on the work of [27]–[29].

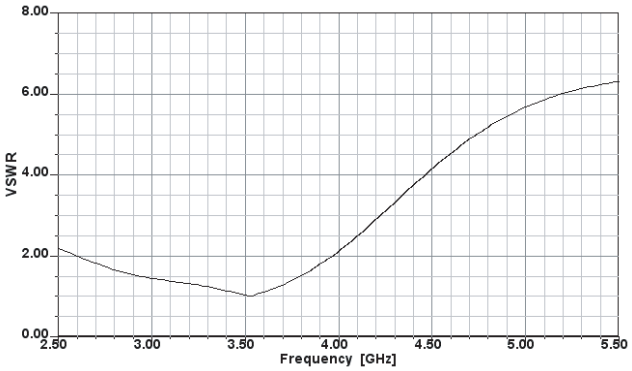

Fig. 4 The antenna VSWR close to the human body.

Table 1 Electrical properties of the human body tissues at 4.1 GHz.

Tissue	ε_r	*σ(S/m)*	*tanδ*
Skin	36.50	2.40	0.29
Fat	5.12	0.19	0.16
Muscle	50.67	3.11	0.27

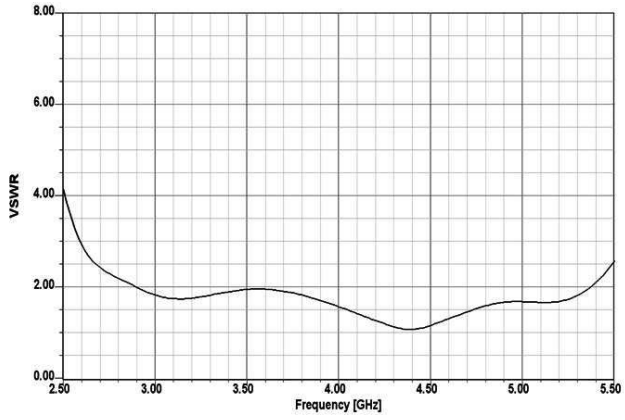

Fig. 5 The antenna VSWR with second substrate layer close to the human body.

The antenna VSWR in the proximity of the above tissue layers and with the appropriate gap from the tissues are shown in Figs. 4 and 5 respectively. It can be seen that in the case of direct contact with tissues, the impedance bandwidth is reduced to 1.4 GHz and the lower frequency is shifted to 2.6 GHz. However, the VSWR of the antenna in proximity of human body with second substrate layer shows the same level of measured VSWR.

3. A 3D Visualization Platform for Wearable and Implantable Sensor

Virtual environments have been previously developed to support a wide range of collaborative activities such as gam-

ing, and few multi-dimensional engineering designs. Here, we present a state of art immersive platform that is applicable for RF propagation study in wireless body area networks.

Figure 6 shows the block diagram of our simulation system. As observed, the main components of this system include: a three-dimensional human body model, the propagation engine which is a three-dimensional full-wave electromagnetic field simulator (i.e., HFSS: High Frequency Structure Simulator) and the 3D immersive & visualization platform. The 3D human body model includes frequency dependent dielectric properties of more than 300 parts in a male human body. These properties are also user-definable if custom changes or modifications are desired. The human body model has a resolution of 2 mm. The HFSS propagation engine enables us to compute a variety of different electromagnetic quantities such as the magnitude of electric and magnetic fields Poynting vectors, and Specific Absorption Rate (SAR).

The 3D immersive platform [30] as shown in Fig. 7 includes several components: three orthogonal screens that provide the visual display, the motion tracked stereoscope glasses, and the hand-held motion tracked input device. The screens are large projection video displays that are placed edge-to-edge in a corner configuration. These three screens are used to display a single three-dimensional stereo scene. The scene is updated based on the position of the user as determined by the motion tracker. This allows the system to present to the user a 3D virtual world within which the user can move and interact with the virtual objects. The main interaction device is a hand-held three button motion-tracked wand with a joystick.

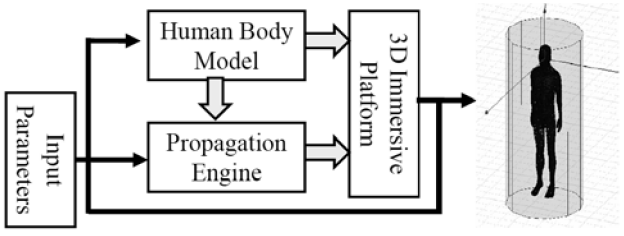

Fig. 6 System block diagram.

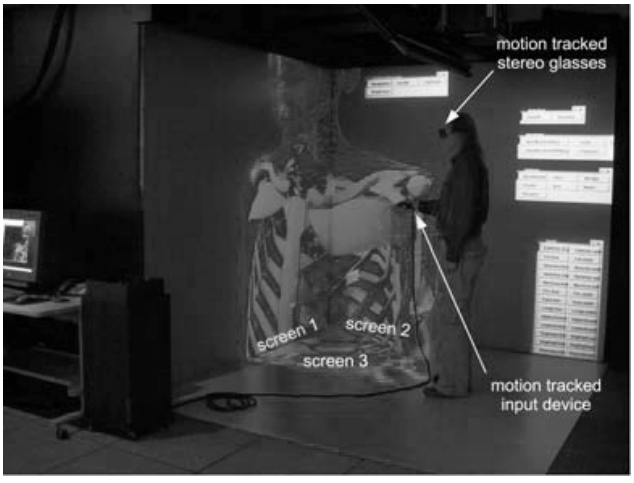

Fig. 7 A user at the immersive visualization environment.

4. Simulation Scenarios and Results

The relative positions of the receivers and transmitters are shown in Fig. 8. The receiver positions are marked with circles while the transmitter positions are marked with a box. The receiver locations have been chosen accordingly to their potential medical application as suggested in [31]. They are left lower arm, left upper arm, left ear, head, right ear, shoulder, chest, right rib and left waist.

The transmitter locations have been chosen according to potential placement of a gateway node such as a cell phone, Personal Digital Assistant (PDA) or a smart watch. They are stomach, right waist and left wrist. In all cases the transmitter antennas were located about 14 mm away from the body surface as shown in Fig. 3.

For each receiver location, the frequency response of the channel was calculated across the UWB frequency range of 3.1 to 5.1 GHz with a step size of 10 MHz. Figure 9 displays all 9 frequency responses corresponding to the 9 receiver locations in Fig. 8(a).

As observed, all channel responses are highly frequency dependent. Using Inverse Fast Fourier Transform (IFFT) with appropriate hamming window, we can obtain the temporal response of the channel.

Figure 10 represents the normalized impulse response of the channel when the receiver is located on the right shoulder. The delay of the first arrival corresponds to the distance traveled by the UWB pulse. To calculate the distance based on the time of arrival, the exact speed of RF waves is needed. In this case, the velocity of RF wave is lower than that of free space (i.e. 3×10^8 m/s). The velocity is reduced by the square root of the permittivity of the body surface since relative permeability is close to 1. For example, for skin (i.e. dielectric permittivity of 36.5 at 4.1 GHz),

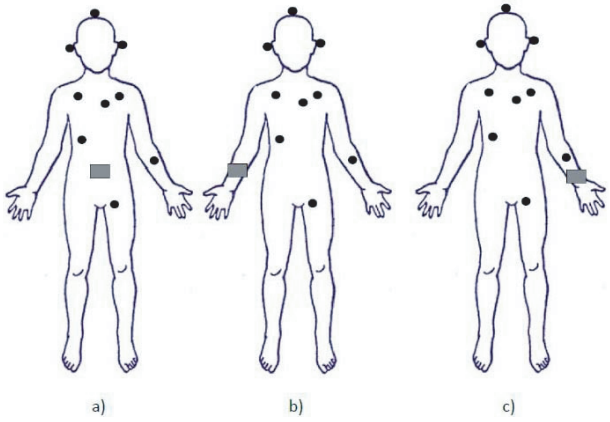

Fig. 8 Various receivers locations for path loss calculation (a) transmitter on stomach (b) transmitter on right-side waist (c) transmitter on the left wrist.

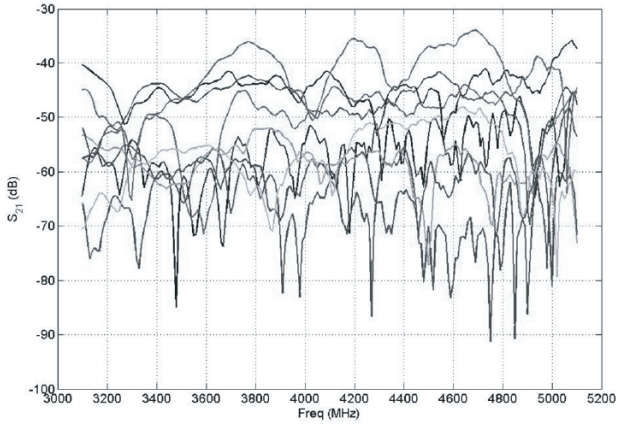

Fig. 9 Channel response in frequency domain for the 9 receive locations.

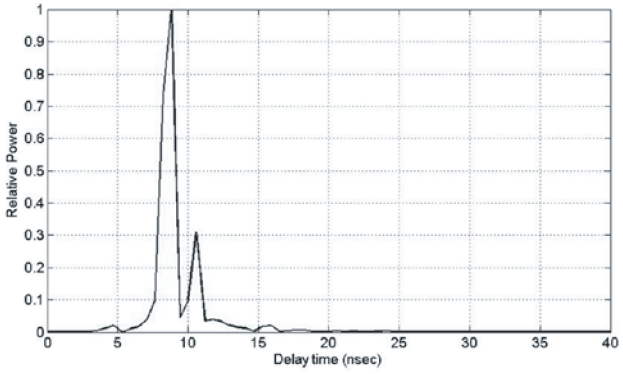

Fig. 10 Impulse response: Stomach to right shoulder.

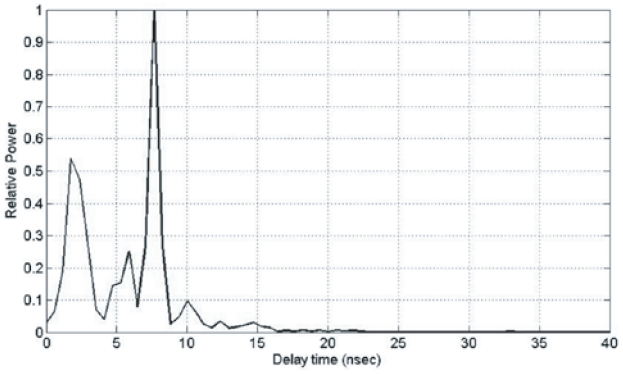

Fig. 11 Impulse response: left wrist to left waist.

the velocity of RF waves is approximately reduced by a factor of 6. As shown in Fig. 10, this translates to a distance of about 40 cm (i.e. 8 ns × (3 × 10^8 m/s)/6) which happens to match the physical straight-line distance (i.e. 40.9 cm) between the transmitter and receiver in this case. In general, derivation of the distance based the arrival times is complicated as the exact speed of RF waves is hard to estimate for body surface propagation.

Figure 11 shows the normalized impulse response of the channel when the receiver is located on the left wrist and the transmitter is located on the left waist. The two arrival components for this scenario possibly correspond to propagation through the air and propagation over the body surface.

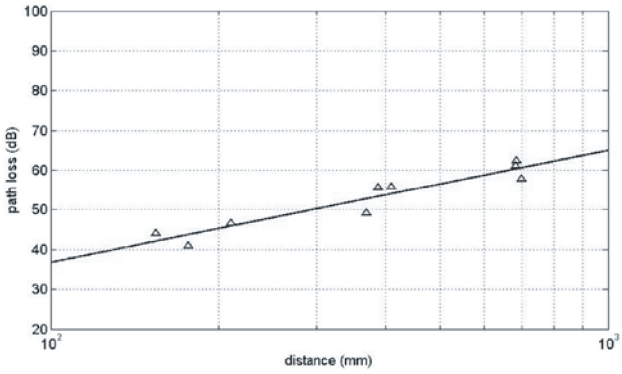

Fig. 12 Path loss versus distance for the 9 points averaged over 3.1–5.1 GHz.

Table 2 Parameters for the statistical path loss model for different transmitter locations.

Transmitter Locations	*PL(d_0) (dB)*	*n*	*σ_s(dB)*
Stomach	28.22	2.83	2.40
Right Waist	26.01	2.85	3.52
Left wrist	18.90	2.98	3.70

The path-loss is calculated between each receiver and the transmitter in Fig. 8(a) at each frequency in the range 3.1–5.1 GHz. The path-loss simply denotes the difference between the transmitted and received power; and therefore, it includes the antenna gains on both side. This is usually not the case for channel models corresponding to most wireless systems, but for BAN, the antenna gains are considered to be part of the channel [1]. This is due to the effect of the body tissues on the antenna characteristics which makes its separation almost impossible.

The path-loss has been characterized by the following statistical model.

$$PL(d) = PL(d_0) + 10n\log_{10}\left(\frac{d}{d_0}\right) + S \text{ (dB)},\ d \geq d_0 \qquad (1)$$

where d_0 is the reference distance (i.e., 50 mm), and n is the path-loss exponent which heavily depends on the environment where RF signal is propagating through. S is the random scatter around the mean and represents deviation in dB caused by different receiver/transmitter positions on the body and their antenna gains in different directions.

The path-loss exponent varies from 0.95 to 5.25 across the frequency band of 3.1–5.1 GHz. The average path-loss for each receiver location and the linear regression line for scenario 'a' of Fig. 8 are shown in Fig. 12.

The random scatters around the mean exhibit a Normal

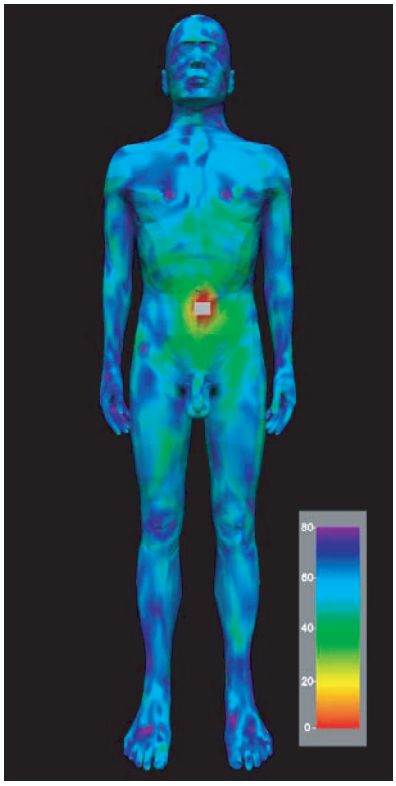

Fig. 13 Path-loss over the body surface when the transmitter is located on the stomach.

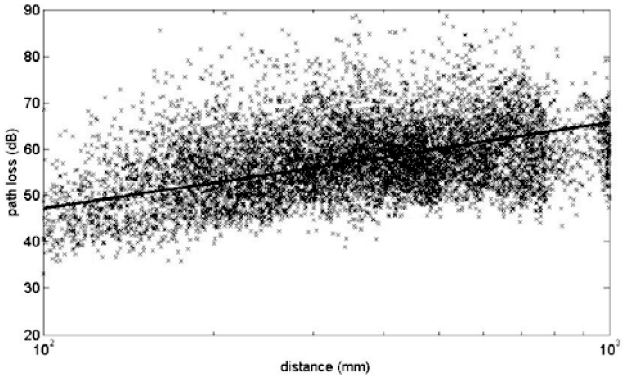

Fig. 14 Scatter plot of the path-loss versus distance for body surface at 4.1 GHz when transmitter is located on the stomach.

distribution with a standard deviation (σ_s) of about 2.4 dB, (i.e. $S \sim N(0, \sigma_s^2)$).

The obtained average path-loss exponent is 2.83 which is roughly in agreement with the physical experiment results reported in [8], [9]. The slight difference could be due to the different antennas used in those studies and the UWB antenna that we have used in our simulation. We repeated our analyses for cases where transmitter was located at different positions (i.e. scenarios 'b' and 'c' of Fig. 8). The extracted path-loss parameters are shown in Table 2. No significant variation in the average path-loss exponent is observed.

In the above process, the derivation of the path-loss pa-

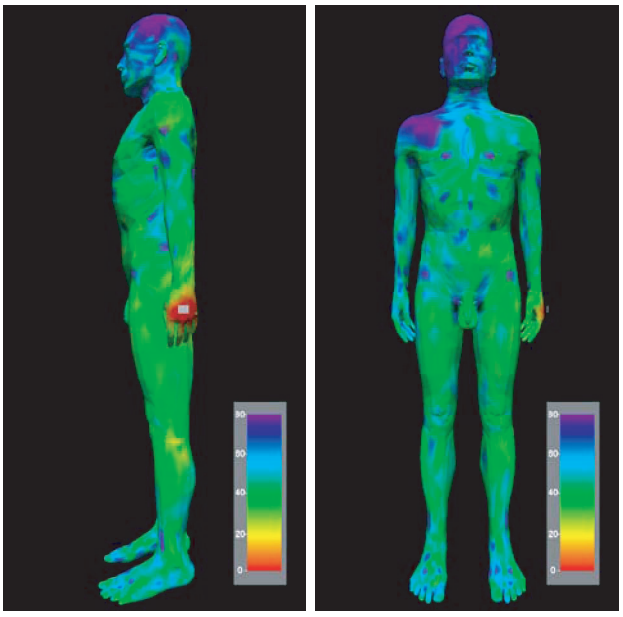

Fig. 15 Path-loss over the body surface when the transmitter is located near the left wrist.

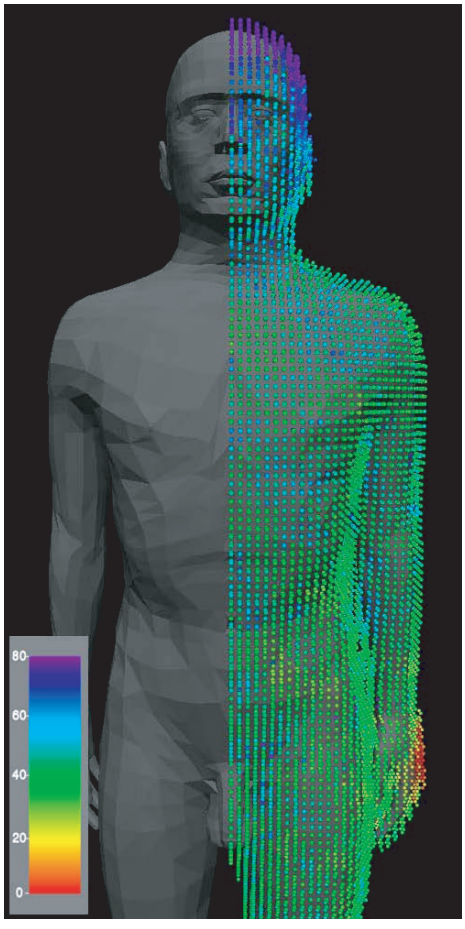

Fig. 16 Sample points that reside on the left-side of the body.

rameters only involved 9 sample points. It is interesting to find out whether more number of sample points affect the resulting parameters. This could be generally difficult to ascertain with more physical experiment as it involves human subjects that have to stand still while participating in the experiment. However, we can easily consider the entire body surface and obtain a comprehensive scatter plot.

Figure 13 shows the path-loss over the entire body surface in the virtual reality platform when the transmitter is located on top of the stomach area.

To obtain the path-loss parameters, here, we have only considered the front side of the body. Since distance should denote over the body-surface distance as opposed to the straight line distance. This is because, at high frequencies, such as UWB, the through-body propagation is almost negligible; and therefore, we only need to consider over-the-surface propagation. This corresponds to over-the-surface distance between a transmitter and a receiver. As measuring the distance between two points over the surface of the body (i.e. a 3D manifold) is not a trivial task, we have filtered out the sample points that are located in the back side of the body and used the approximation of straight-line distance for all sample points that are in the front side of the body.

Figure 14 shows the scatter plot for the path-loss at 4.1 GHz as a function of TX-RX separation for the case when the transmitter is located on the stomach.

The mean value of the random path-loss has been displayed by a solid line. This is obtained by fitting a least squares linear regression line through the scatter of measured path-loss sample points in dB such that the root mean square deviation of sample points about the regression line is minimized. As shown in Fig. 12, this random scatters around the mean still shows a normal distribution with zero mean and standard deviation of about 8.34 dB. The path loss exponent has been reduced to 1.87.

We repeated our analyses for the scenarios 'b' and 'c' where transmitter was located at different positions. Figure 15 shows the path-loss on the body surface when the transmitter is located near the left wrist.

Keeping in mind that in order to have the right estimation for sample point distances, only the points that reside on the left side of the body has been used, as shown in Fig. 16.

The extracted path-loss parameters for the scenarios where transmitter is located on the right waist and left wrist are shown in Table 3.

As shown in Table 4, the path-loss exponent is lower in all cases compared to the case with 9 sample points. The reason could be due to existence of creeping waves around the body surface. With help of 3D immersive platform we have observed that the directions of the Poynting vectors which represent the direction of energy flux of an electromagnetic field are mostly parallel to the body surface. This creeping wave phenomenon could facilitate the propagation of RF waves over the body surface; and therefore, lead to a better loss exponent for on-body channels.

Table 3 Parameters for the statistical path loss model for different transmitter locations at 4.1 GHz.

Transmitter Locations	*PL(d_0) (dB)*	*n*	*σ_s(dB)*
Stomach	41.53	1.87	7.94
Right Waist	32.12	2.10	9.51
Left wrist	25.24	1.91	9.72

Table 4 Parameters for the statistical path loss model for different frequencies.

Frequency (GHz)	*PL(d_0) (dB)*	*n*	*σ_s(dB)*
3.3	45.77	1.64	8.34
4.1	41.53	1.87	7.94
4.7	38.57	1.40	7.87

5. Conclusion

A 3D virtual reality simulation environment has been used for investigation of body-surface propagation for body area network. In particular, the parameters of statistical path-loss model and how they are affected when the number or location of the sample points changed.

One difficulty in comparing the results of such simulations with actual measurements or even comparing the results of two sets of measurements data obtained by two different sources is the inclusion of the antenna characteristics in the channel model.

In general, studying body surface propagation for specific scenarios such as people wearing medical implant is also possible with this platform. Also, evaluating the efficiency of custom made antennas and comparing the results with other antennas can be easily done in our system.

More in-depth research on this subject is undoubtedly required to further understand the characteristics of radio frequency propagation for wearable sensors. The authors hope that the virtual reality environment introduced here would create a flexible platform to visualize and understand body surface propagation without the need for extensive measurement campaign.

References

[1] G. Yang, Body sensor networks, Springer-Verlag London Limited, ISBN 1-84628-272-1, 2006.
[2] D. Porcino and W. Hirt, "Ultra-wideband radio technology: Potential and challenges ahead," IEEE Commun. Mag., vol.41, no.7, pp.66–74, July 2003.
[3] M. Billinghurst and T. Starner, "Wearable devices: New ways to manage information," Computer, vol.32, no.1, pp.57–64, Jan. 1999.

[4] K. Yekeh Yazdandoost and R. Kohno, "Design and analysis of an antenna for ultra-wideband system," 14th IST Mobile and Wireless Communications Summit, 2005.
[5] W.-T. Chen and H.-R. Chuang, "Numerical computation of human interaction with arbitrarily oriented superquadric loop antennas in personal communications," IEEE Trans. Antennas Propag., vol.46, no.6, pp.821–828, June 1998.
[6] K. Takizawa, T. Aoyagi, J. Takada, N. Katayama, K.Y. Yazdandoost, T. Kobayashi, and R. Kohno, "Channel models for wireless body area networks," Proc. 30th Annual International IEEE EMBS Conference, Aug. 2008.
[7] A. Fort, J. Ryckaert, C. Desset, P. Doncker, P. Wambacq, and L.V. Biesen, "Ultra-wideband channel model for communication around the human body," IEEE J. Sel. Areas Commun., vol.24, no.4, April 2006.
[8] A. Fort, C. Desset, J. Ryckaert, P.D. Doncker, L.V. Biesen, and P. Wambacq, "Characterization of the ultra wideband body area propagation channel," Proc. ICU, pp.22–27, Zurich, Switzerland, 2005.
[9] T. Zasowski, F. Althaus, M. Stager, A. Wittneben, and G. Troster, "UWB for noninvasive wireless body area networks: Channel measurements and results," Proc. IEEE Conference on Ultra Wideband System and Technoloy, pp.285–289, Nov. 2003.
[10] K.L. Wong, G.Y. Lee, and T.W. Chiou, "A low-profile planar monopole antenna for multiband operation of mobile handsets," IEEE Trans. Antennas Propag., vol.51, pp.121–125, Jan. 2003.
[11] J. Perruisseau-Carrier, T.W. Hee, and P.S. Hall, "Dual-polarized broadband dipole," IEEE Antennas Wireless Propag. Lett., vol.2, pp.310–312, 2003.
[12] R.L. Li, E.M. Tentzeris, J. Laskar, V.F. Fusco, and R. Cahill, "Broadband loop antenna for DCS-1800/IMT-2000 mobile phone handsets," IEEE Microw. Wireless Compon. Lett., vol.12, pp.305–707, Aug. 2002.
[13] K.D. Katsibas, C.A. Balanis, P.A. Tirkas, and C.R. Birtcher, "Folded loop antenna for mobile hand-held units," IEEE Trans. Antennas Propag., vol.46, pp.260–266, Feb. 2003.
[14] R.L. Li and V.F. Fusco, "Circularly polarized twisted loop antenna," IEEE Trans. Antennas Propag., vol.50, pp.1377–1381, Oct. 2002.
[15] K. Yekeh Yazdandoost and R. Kohno, "Ultra wideband L-loop antenna," IEEE International Conference on Ultra-Wideband, pp.201–205, 2005.
[16] Z.N. Chen and M.Y.W. Chia, "Broadband planar inverted-L antennas," IEE Proc. Microwaves, Antennas and Propagation, vol.148, pp.339–342, Oct. 2001.
[17] Z.N. Chen and M.Y.W. Chia, "Suspended plate antenna with a pair of L-shaped strips," IEEE APS Symposium, vol.3, pp.64–67, June 2002.
[18] W.L. Stutzman and G.A. Thiele, Antenna Theory and Design, second ed., John Wiley & Sons, NY, 1998.
[19] S. Yamamoto, T. Azakami, and K. Itakura, "Coupled nonuniform transmission line and its applications," IEEE Trans. Microw. Theory Tech., vol.15, pp.220–231, April 1967.
[20] O.P. Rustogi, "Linearly tapered transmission line and its application in microwaves," IEEE Trans. Microw. Theory Tech., vol.17, pp.166–168, March 1969.
[21] N.M. Martin and D.W. Griffin, "A tapered transmission line model for the feed-probe of a microstrip patch antenna," IEEE APS Symposium, vol.21, pp.154–157, May 1983.
[22] I. Smith, "Principles of the design of lossless tapered transmission line transformers," 7th Pulsed Power Conference, pp.103–107, June 1989.
[23] Y. Wang, "New method for tapered transmission line design," Electron. Lett., vol.27, pp.2396–2398, Dec. 1991.
[24] K. Murakami and J. Ishii, "Time-domain analysis for reflection characteristics of tapered and stepped nonuniform transmission lines," Proc. IEEE International Symposium on Circuits and Systems, vol.3, pp.518–521, June 1998.
[25] K. Yekeh Yazdandoost and R. Kohno, "UWB antenna for wireless body area network," Asia Pacific Microwave Conference, pp.1647–1650, Dec. 2006.
[26] http://www.cumingcorp.com/microdm.php
[27] C. Gabriel and S. Gabriel, "Compilation of the dielectric properties of body tissues at RF and microwave frequencies," AL/OE-TR-1996-0037, June 1996, http://www.brooks.af.mil/AFRL/HED/hedr/reports/dielectr-icReport/Report.html
[28] C.H. Duney, H. Massoudi, and M.F. Iskander, "Radiofrequency radiation dosimetry handbook," USAF School of Aerospace Medicine, Oct. 1986.
[29] Italian National Research Council, Institute for Applied Physics, "Dielectric properties of body tissues," http://niremf.ifac.cnr.it http://www.cumingcorp.com/microdm.php
[30] J.G. Hagedorn, J.P. Dunkers, S.G. Satterfield, A.P. Peskin, J.T. Kelso, and J.E. Terrill, "Measurement tools for the immersive visualization environment: Steps toward the virtual laboratory," J. Research of the National Institute of Standard & Technology, vol.112, no.5, Sept.-Oct. 2007.
[31] K. Takizawa, T. Aoyagi, J. Takada, N. Katayama, K. Yekeh Yazdandoost, T. Kobayashi, and R. Kohno, "Channel models for wireless body area networks," Proc. 30th Annual International IEEE EMBS Conference, Aug. 2008.

Kamya Yekeh Yazdandoost received his Ph.D. degree from University of Pune, India. He joined the Communications Research Laboratory (CRL), Japan in 2003 (now, National Institute of Information and Communications Technology: NICT), and has been engaged in research on Ultra WideBand (UWB) and Wireless Body Area Network (BAN) technology. He is currently working as an Expert Researcher at the Medical-ICT group, National Institute of Information and Communications Technology, Japan. Dr. Yazdandoost is an adjunct Professor at University of Oulu, Finland and he is the recipient of Finland Distinguished Professor Program (FIDIPRO) for the periods of 2010–2014. From May 2001 to May 2003 he was with the Department of Microsystem Engineering, Nagoya University, Japan, as a Japan Society for the Promotion of Science (JSPS) Research Fellow. He was invited Guest Professor at the Asian Institute of Technology in Bangkok Thailand Feb. 2007. He is the Chair of the channel modeling committee and the co-editor of the channel modeling document of the IEEE.802.15.6 on Body Area Network Standardization. He is a representative of the NICT to the European COST2100 Action (Management Committee Meeting on Pervasive Mobile and Ambient Wireless Communications). He is a member of IEEE and a life member of the IEEE Microwave Theory and Techniques Society. He is also a Member of European Microwave Association. He is holding six patents and his four other patents are pending. He is also Associate Editor of International Journal of Microwave Science and Technology and served as invited guest editor of many international Journals. He has been the TPC member and session chair of various international conferences. He is the recipient of the IEEE PIMRC 2009 best paper award. He is listed in the Who's Who in Science and Engineering and the Who's Who in the World 2006, 2007, 2008, and 2009. He has published over 50 conference and journal papers, and book chapters. His research interests include antenna, on-body and implantable antenna, body area networks, medical implant communication systems, SAR and EMC.

Kamran Sayrafian-Pour is a program manager at the Information Technology Laboratory of the National Institute of Standard and Technology (NIST) located in Gaithersburg, Maryland. He holds Ph.D., M.S. and B.S. degrees in Electrical & Computer Engineering from University of Maryland, Villanova University and Sharif University of Technology, respectively. Prior to joining NIST, he was the cofounder of Zagros Networks, Inc. a fables semiconductor company based in Rockville, Maryland where he served as President and senior member of the architecture team. Dr. Sayrafian is the co-inventor/inventor of four U.S. patents. He is a senior member of IEEE and an adjunct faculty of the University of Maryland. He has served as invited member of technical program committees of many international conferences and also the technical advisory board of a DARPA program. His research interests include body area networks, medical implant communication systems, mobile sensor networks and RF-based indoor positioning. He has published over 40 conference and journal papers, and book chapters in these areas. He is the recipient of the IEEE PIMRC 2009 best paper award. He has also been a contributing member and the co-editor of the channel modeling document of the IEEE802.15.6 international standardization on body area networks.

Kiyoshi Hamaguchi received the B.S. and M.S. degrees in electrical engineering from Science University of Tokyo in 1989 and 1991, respectively. He also received the Ph.D. degree in electrical engineering from Osaka University in 2000. Since 1993 he has been with the National Institute of Information and Communications Technology (NICT), Japan, where he has been engaged in research and development on wireless telecommunication systems. From 2002 to 2003, he was a visiting researcher at University of Southampton, U.K. He received the Young Engineer Award from IEICE in 1997, the Young Scientist Award from Ministry of Education, Culture, Sports, Science and Technology of Japan in 2006 and the Radio Achievement Award from the Association of Radio Industries and Businesses (ARIB) in 2010. He is currently a group leader of Medical ICT group in NICT.